PCCP

RSC Publishing

PAPER

View Article Online
View Journal | View Issue

Cite this: *Phys. Chem. Chem. Phys.*, 2013, **15**, 5395

Probing the dielectric response of graphene *via* dual-band plasmonic nanoresonators

Ye Xiao,*[a] Yan Francescato,*[a] Vincenzo Giannini,[a] Mohsen Rahmani,[b] Tyler R. Roschuk,[a] Adam M. Gilbertson,[a] Yannick Sonnefraud,[a] Cecilia Mattevi,[c] Minghui Hong,[d] Lesley F. Cohen[a] and Stefan A. Maier[a]

Received 2nd November 2012,
Accepted 28th January 2013

DOI: 10.1039/c3cp43896a

www.rsc.org/pccp

In this article, we use optical transmission spectroscopy to measure the changes in the resonance features of a Au plasmonic nanoresonator array consisting of concentric ring/disc cavity elements, when graphene is introduced as an encapsulating medium. We show that by using finite element modelling to best reproduce our experimental results the dielectric response of the graphene film can be determined. We discuss the potential of such structures for chemical sensing applications.

Introduction

The integration of graphene with plasmonic devices offers opportunities for the development of planar optoelectronic devices[1,2] and highly integrated chemical sensors.[3] The potential for future applications lies in the highly desirable electronic properties of graphene, such as high carrier mobility[4] and a tuneable Fermi energy level,[5] as well as the recent demonstration of scalable large area synthesis and fabrication.[6] Combining this with the ability to manipulate light at the nanoscale, as well as the field enhancement possibilities offered by plasmonics, provides a possible route to overcoming the current problems in Si based integrated photonics such as downscaling as well as making use of higher order non-linear optical effects.[7,8] Paramount to this effort is the need to better explore the optical response of plasmonic nanoresonators coupled to graphene at frequencies beyond the visible spectrum.

Whilst graphene has been shown to exhibit a universal optical conductivity in the visible regime,[9] this is not the case in the mid-IR where a clear frequency dependency arises.[10,11] It is well known that graphene's conductivity can be defined by the Kubo formula[12] in the local random phase approximation (RPA).[13–15] An interesting property of graphene is that its dielectric constant can be tuned by electrostatic gating as recently shown by ref. 16. As such, the interaction between a graphene monolayer and a plasmonic array in intimate contact is largely affected by the Fermi energy of the sheet, as well as its defect density. In this paper, we examine the effects of a graphene overlayer on the localized surface plasmon resonance (LSPR) of a Au nanoresonator array, consisting of concentric ring/disc cavity (CRDCs) elements,[17] chosen for their hybridized mode spectrum with two distinct sub- and super-radiant dipolar modes. We demonstrate that the shift in the LSPR can be used to determine the dielectric properties of the graphene. Furthermore, we use finite element method simulations to investigate sensitivity of the LSPR modes to changes in the chemical potential of the graphene overlayer.

Experimental

Sample fabrication

Au CRDCs of 60 nm thickness arranged on a square grid with a periodicity of 3 μm were fabricated on a quartz substrate by top down approach using e-beam lithography (Elonix 100KV EBL system) and a subtractive etch. First, a Ti(3 nm)/Au(60 nm) thick film (Ti was used as an adhesion layer) was deposited onto the substrate by e-beam evaporation (EB03 BOC Edwards). Negative tone e-beam resist, Hydrogen Silses Quioxane (HSQ), was spun onto the sample and patterned to define the etch mask. Finally, an ion-milling process was established to create well-defined Au nanostructures on the substrate. Fig. 1a shows an SEM image of the CRDC array, the inset shows the typical structure of one of the CRDC elements found within the array.

[a] *Blackett Laboratory, Imperial College London, Prince Consort Road, London, SW7 2BZ, UK. E-mail: ye.xiao@ic.ac.uk, yan.francescato10@ic.ac.uk; Tel: +44 (0)2075 947 627*
[b] *Data Storage Institute, (A* STAR) Agency for Science, Technology and Research, 5 Engineering Drive 1, Singapore 117608. E-mail: mohsenrahmani.82@gmail.com*
[c] *Materials Department, Imperial College London, Prince Consort Road, London, SW7 2AZ, UK. E-mail: c.mattevi@ic.ac.uk*
[d] *Department of Electrical and Computer Engineering, National University of Singapore, Singapore 117576. E-mail: elehmh@nus.edu.sg*

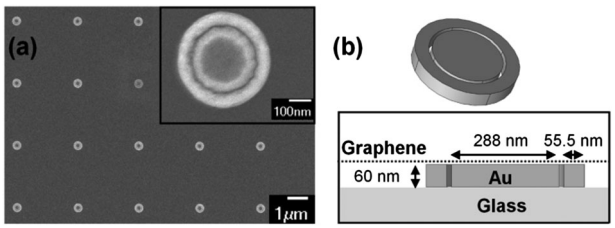

Fig. 1 (a) SEM image of the CRDC array. The inset shows a close up of an individual ring-disc element (b) schematic of the simulated CRDC structure with cross section shown. The ring has an outer diameter of 425 nm and an inner diameter of 314 nm, the disk has a diameter of 288 nm, the gap between ring and disk is 13 nm and both structures are 60 nm tall.

Graphene grown on Cu by chemical vapour deposition was purchased from Graphene-Supermarket. A thin layer of PMMA was spun on top of the graphene film. The Cu substrate was removed using a $FeCl_3$ wet chemical etch and the graphene film was transferred onto our CRDC array using HCl, H_2O and acetone. A more detailed description of the transfer process can be found in ref. 18.

Spectroscopy

Transmittance (Tr) curves of both the bare and encapsulated array were obtained at normal incidence with a Bruker Hyperion 2000 Fourier transform infrared (FTIR) microscope with a 36×, NA = 0.5 microscope objective. Spectra were obtained in the ranges 1.4–0.6 eV and 0.7–0.4 eV using a Peltier cooled InGaAs detector and a liquid nitrogen cooled MCT detector respectively. The illuminated sample area was approximately $50 \times 50\ \mu m^2$. Transmittance curves were obtained after normalization by a reference spectrum taken from an area next to the array. Extinction spectra were defined as (1-Tr).

Raman characterisation of the graphene film was performed with a Renishaw 2000 spectrometer with an attached Leica DMLM confocal microscope and a 50× objective. All Raman measurements were taken with 514 nm excitation scanning from 1000–3000 cm^{-1} with a 10 s integration time. Raman mapping was performed over a $49 \times 49\ \mu m^2$ area across the CRDC array with a 7 μm resolution in both x and y directions.

FEM simulations

Simulations were performed using the finite element method with the commercial package Comsol. The dielectric function used for gold was obtained from a four Lorentzian expression.[19] The simulated structure, shown in Fig. 1b, takes its dimensions from the SEM image whilst the height was confirmed using atomic force microscopy. The structure was modelled with an infinitely thick glass substrate with Fresnel reflections at the air/substrate interface accounted for. The graphene layer was modelled as a boundary condition, defined by current density, lying directly on top of our CRDC structure. The surface current density was defined by the cross product of the complex conductivity with the incident field such that $\vec{J} = \mathrm{Im}(\vec{\sigma}) \times \vec{E}_{\mathrm{incident}}$. The complex conductivity for graphene was obtained from the local RPA approximation of the Kubo formula which leads to

$$\sigma = \sigma_{\mathrm{intra}} + \sigma_{\mathrm{inter}} \quad (1)$$

$$\sigma_{\mathrm{intra}} = \frac{2ie^2T}{\hbar^2\pi(\omega + i\Gamma)}\ln\left[2\cosh\left(\frac{\mu}{2T}\right)\right] \quad (2)$$

$$\sigma_{\mathrm{inter}} = \frac{e^2}{4\hbar}\left[\frac{1}{2} + \frac{1}{\pi}\arctan\left(\frac{\hbar\omega - 2\mu}{2T}\right) - \frac{i}{2\pi}\ln\frac{(\hbar\omega - 2\mu)^2}{(\hbar\omega - 2\mu)^2 + (2T)^2}\right] \quad (3)$$

where ω is the angular frequency of light, T the temperature energy, Γ the scattering rate and μ the chemical potential (where μ is equal to the Fermi energy E_f).[20] The complex conductivity is given by $\sigma = \sigma_1 + i\sigma_2$, where $\sigma_1 = \mathrm{Re}(\sigma)$ and $\sigma_2 = \mathrm{Im}(\sigma)$ are the real and imaginary parts of the conductivity. For all simulations the temperature was defined to be 300 K while μ and Γ were used as fitting parameters.

Results and discussion

Raman spectroscopy

The presence of single layer graphene on our sample was confirmed using Raman spectroscopy as well as optical images taken of graphene films, from the same Cu foil, transferred onto SiO_2(300 nm)/Si substrates. Fig. 2 shows the averaged Raman spectrum taken from the graphene film where it lies directly above the Au CRDC array (solid line) as well as on the bare quartz substrate (dashed line). We anticipate the graphene to be p-doped, particularly when directly above the Au CRDC array.[21,22] The carrier density $n(E_f)$ can be estimated from the ratio of the G to 2D peak intensity ($I_{G/2D}$), using the relationship shown in the inset to Fig. 2, following ref. 23. For the measured $I_{G/2D} = 0.49 \pm 0.03$ (on quartz) and 0.8 ± 0.2 (on Au CRDC array)

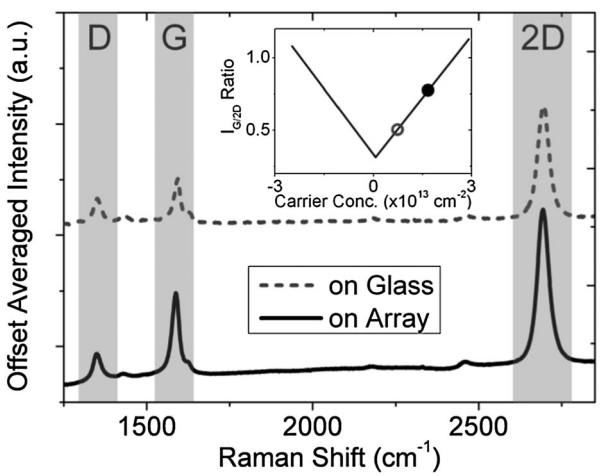

Fig. 2 Averaged Raman spectrum taken of the graphene film on the quartz substrate (dashed line) and directly above the Au CRDC array (solid line). The inset, adapted from ref. 23, shows a schematic response of the $I_{G/2D}$ ratio to changes in the carrier concentration, highlighting the $I_{G/2D}$ ratio from our graphene film when on the bare quartz (open circle) and directly above the Au CRDC array (closed circle).

we estimate a value of $n(E_f) \sim 0.39(\pm 0.06) \times 10^{13}$ cm^{-2} and $1.5(\pm 0.9) \times 10^{13}$ cm^{-2} respectively.

The graphene film also shows a significant D peak, associated with defects, as shown in Fig. 2. Defected graphene has been reported to have a reduced Fermi velocity and we estimate that $\nu_F \sim 5 \times 10^5 \pm 1$ ms^{-1} for our sample based on the $I_{D/2D}$ ratio.[24,25] An estimation of the chemical potential μ can then be made using the Fermi energy equation,[26]

$$n(E_f) = \frac{1}{\pi}\left(\frac{E_f}{\hbar V_f}\right), \quad (4)$$

giving $\mu \sim 120 \pm 20$ meV and 200 ± 100 meV above the bare quartz substrate and the Au CRDC array respectively.

Fourier transform infrared spectroscopy

FTIR spectroscopy was used to capture the extinction spectra of the sample before and after depositing a graphene layer on top. Fig. 3a shows the extinction spectrum of the bare CRDC array, which exhibits two resonance features with peaks at 0.5 and 1.15 eV (solid line). This double resonance can be understood by first considering both the simple ring and disc nanostructure in complete separation from one another. Both individual structures produce dipolar plasmon modes dependent on their respective dimensions. When the disc is placed inside the ring a hybridization of their modes results in either parallel or anti-parallel coupling of their dipolar moments, producing a super- and sub-radiant plasmon mode respectively. The sub-radiant mode has a smaller net dipole moment, due to the anti-parallel coupling, and thus exhibits less radiative losses and, as such, has a higher Q factor compared to the super-radiant mode. A more detailed account of the interactions between the ring and disk parent modes has been given previously.[27]

The addition of a graphene layer to the plasmonic structure produces a redshift for both resonances (dashed line in Fig. 3a). The redshift is observed to be significantly more pronounced for the sub-radiant mode in comparison to the super-radiant mode, ~20 meV and ~70 meV respectively. Moreover, we observe that the Q factor of the sub-radiant mode decreases by ~17% with the introduction of the graphene layer, as the FWHM changes from 67 meV to 83 meV with the addition of graphene in a similar manner to results reported by ref. 16.

Finite element method simulations

Fig. 3b shows our simulated results for a graphene sheet using the value μ = 260 meV, which best reproduces the shifts in the extinction spectra we observe experimentally. The μ value is consistent with the estimates made from the Raman data. We have chosen Γ = 20 meV based on the value reported by ref. 28 for CVD grown graphene.

Similar redshifts of plasmon resonances have been reported, by other groups, with the introduction of graphene.[29–31] This behaviour can be understood by considering the complex conductivity of graphene with real and imaginary parts, σ_1 and σ_2 respectively. In the visible to mid-IR regime both interband and intraband transitions contribute to the conductivity and are closely tied to the chemical potential and temperature.[7,32,33] Fig. 4 shows how the energy dependency of both σ_1 and σ_2 vary with different values of μ as calculated from eqn (1)–(3) with temperature fixed at 300 K. For lightly doped graphene σ_2 is negative over a larger energy range whilst σ_1 remains at its upper limit. The magnitude of σ_1 is related to the absorbance of graphene[34] whilst the sign of σ_2 is important as it determines if the plasmon resonance is red or blue shifted with respect to the bare nanoresonator. This is because σ_2 is related to the dielectric constant of graphene by $\varepsilon = 1 + i\sigma/\omega\varepsilon_0$. Therefore $\mathrm{Im}(\sigma) < 0$ corresponds to $\mathrm{Re}(\varepsilon) > 0$ and vice versa, which in turn determines the effective wavelength of the resonance $\lambda = \lambda_0/\mathrm{Re}(n)$, where λ_0 is the free space wavelength. As such, the graphene should cause both a redshift and damping of the plasmon features. This agrees well with our experimental observations in Fig. 3a.

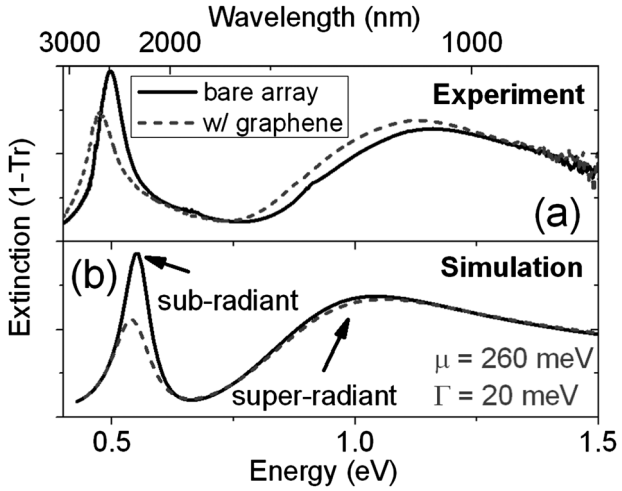

Fig. 3 Extinction spectra of CRDC array before (solid line) and after depositing graphene layer on top (dashed line) for both (a) experimental and (b) simulation with μ = 260 meV and Γ = 20 meV.

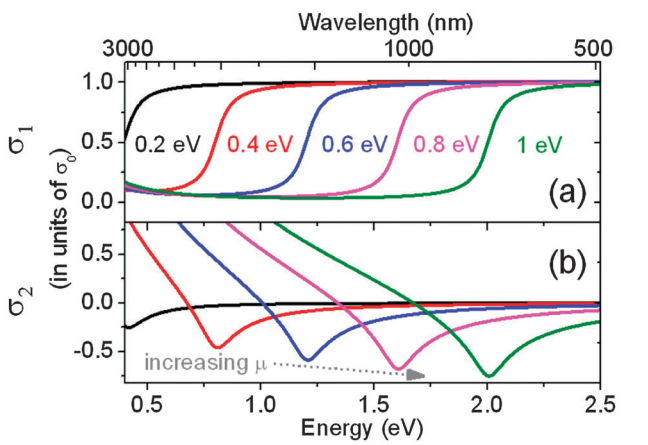

Fig. 4 Excitation energy dependency of both (a) real and (b) imaginary conductivity of graphene for μ = 0.2 eV (black), 0.4 eV (red), 0.6 eV (blue), 0.8 eV (purple), 1 eV (green) with Γ fixed at 20 meV.

Chemical sensing potential

It has been shown that graphene has potential to be used for detection of physisorption of chemicals down to concentrations of 0.1 ppm using electrical methods.[35] The measured change in resistivity at the 0.1 ppm level corresponds to changes in chemical potential $\Delta\mu \sim 0.07$ meV. Although in order to determine the sign of $\Delta\mu$ both longitudinal and transverse resistivity must be measured by four probe methods in both zero and finite applied magnetic fields. Clearly, optical detection offers some advantages in terms of simplicity and speed. In Fig. 5 we show simulated results examining the sensitivity of both super- and sub-radiant modes of our plasmon structure to changes in the chemical potential of the overlaying graphene film (as would be the case if μ were being altered by external gating[31,36] or deliberate chemical doping[22]). As shown in Fig. 5a, for $\mu > 200$ meV, both modes of our plasmon structure become highly sensitive to $\Delta\mu$ (the sub-radiant mode more so, although this is more apparent when the shift in the resonance features is shown in wavelength).

In Fig. 5b we show the peak shift, (the quantity that would be measured explicitly) *versus* μ. The shaded region represents the range most useful for chemical sensing for the current plasmonic structure. The sensor could be easily fabricated on a SiO_2/Si substrate thus allowing biasing *via* a back gate to tune μ to the optimal range. For the structure we have characterised here we believe it would be possible to resolve peak shifts of the order of $\sim$4 meV (18 nm) which would be equivalent changes in the chemical potential $\Delta\mu$ in the $\sim$25 meV range. We note that whilst the sensitivity of our device will not meet the requirement for single molecular detection,[35] improvements in sensitivity could be made by altering the design of the array and the choice of plasmonic metal so that parts per million detection levels might be achieved. Moreover, as the sub-radiant mode has a non-monotonic change with μ, differentiation of p- and n-type doping can be made by simultaneously tracking the shift of the super-radiant mode. Indeed examining differential changes between these two modes may lead to a more robust detection scheme. In addition, for some chemical potential ranges the two modes will shift in the opposite sense as highlighted in the inset to Fig. 5b which may indeed facilitate additional sensitivity. We find these results demonstrate encouraging potential for chemical sensor applications and believe that there is plenty of scope to improve sensitivity by at least an order of magnitude over the structure we have studied here.

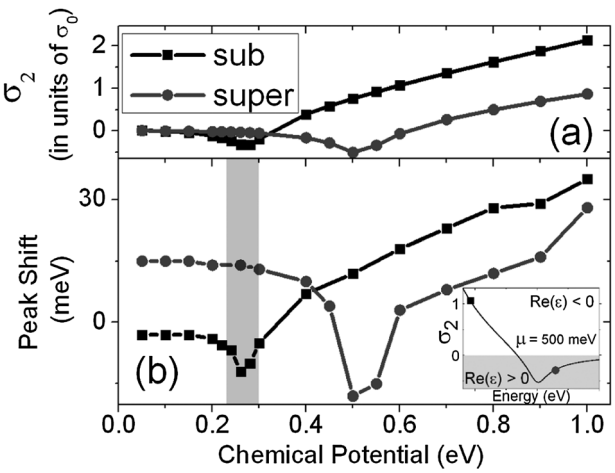

Fig. 5 (a) The values of σ_1 and σ_2 at the super- (circles) and sub-radiant (squares) modes for a graphene sheet with different values of μ and Γ = 20 meV (b) shift in the resonance of both super- (circles) and sub- (squares) radiant modes at various different values of μ with Γ = 20 meV. Inset shows σ_2, for μ = 500 meV and Γ = 20 meV, highlighting the sign change from the super- (circle) to sub-radiant (square) resonance.

Conclusions

In summary we have shown that changes in plasmon resonance energies of Au nanocavity arrays can be used to determine the dielectric properties of graphene with good accuracy when the experimental changes in resonance structures are compared to a finite element model of the graphene optical properties. We further show the attraction of using the hybridised double resonance plasmonic structure for future chemical sensing applications.

Acknowledgements

We would like to thank the UK EPSRC for funding this work through the S&I grant EP/D063329, and the Leverhulme Trust.

Notes and references

1 T. J. Echtermeyer, L. Britnell, P. K. Jasnos, A. Lombardo, R. V. Gorbachev, A. N. Grigorenko, A. K. Geim, A. C. Ferrari and K. S. Novoselov, *Nat. Commun.*, 2011, **2**, 458.
2 Z. Fang, Z. Liu, Y. Wang, P. M. Ajayan, P. Nordlander and N. J. Halas, *Nano Lett.*, 2012, **12**, 3808–3813.
3 J. C. Reed, H. Zhu, A. Y. Zhu, C. Li and E. Cubukcu, *Nano Lett.*, 2012, **12**, 4090–4094.
4 K. I. Bolotin, K. J. Sikes, Z. Jiang, M. Klima, G. Fudenberg, J. Hone, P. Kim and H. L. Stormer, *Solid State Commun.*, 2008, **146**, 351–355.
5 Y.-J. Yu, Y. Zhao, S. Ryu, L. E. Brus, K. S. Kim and P. Kim, *Nano Lett.*, 2009, **9**, 3430–3434.
6 S. Bae, H. Kim, Y. Lee, X. Xu, J.-S. Park, Y. Zheng, J. Balakrishnan, T. Lei, H. Ri Kim, Y. I. Song, Y.-J. Kim, K. S. Kim, B. Ozyilmaz, J.-H. Ahn, B. H. Hong and S. Iijima, *Nat. Nanotechnol.*, 2010, **5**, 574–578.
7 Q. Bao and K. P. Loh, *ACS Nano*, 2012, **6**, 3677–3694.
8 V. Giannini, A. I. Fernández-Domínguez, S. C. Heck and S. A. Maier, *Chem. Rev.*, 2011, **111**, 3888–3912.
9 R. R. Nair, P. Blake, A. N. Grigorenko, K. S. Novoselov, T. J. Booth, T. Stauber, N. M. R. Peres and A. K. Geim, *Science*, 2008, **320**, 1308.
10 F. T. Vasko and V. Ryzhii, *Phys. Rev. B: Condens. Matter Mater. Phys.*, 2008, **77**, 195433.

11 F. H. L. Koppens, D. E. Chang and F. J. Garcia de Abajo, *Nano Lett.*, 2011, **11**, 3370–3377.
12 A. Vakil and N. Engheta, *Science*, 2011, **332**, 1291–1294.
13 B. Wunsch, T. Stauber, F. Sols and F. Guinea, *New J. Phys.*, 2006, **8**, 318.
14 E. H. Hwang and S. Das Sarma, *Phys. Rev. B: Condens. Matter Mater. Phys.*, 2007, **75**, 205418.
15 L. A. Falkovsky, *Phys.–Usp.*, 2008, **51**, 887.
16 J. Kim, H. Son, D. J. Cho, B. Geng, W. Regan, S. Shi, K. Kim, A. Zettl, Y.-R. Shen and F. Wang, *Nano Lett.*, 2012, **12**, 5598–5602.
17 F. Hao, P. Nordlander, Y. Sonnefraud, P. V. Dorpe and S. A. Maier, *ACS Nano*, 2009, **3**, 643–652.
18 C. Mattevi, H. Kim and M. Chhowalla, *J. Mater. Chem.*, 2011, **21**, 3324–3334.
19 F. Hao and P. Nordlander, *Chem. Phys. Lett.*, 2007, **446**, 115–118.
20 V. P. Gusynin, S. G. Sharapov and J. P. Carbotte, *J. Phys.: Condens. Matter*, 2007, **19**, 026222.
21 I. Gierz, C. Riedl, U. Starke, C. R. Ast and K. Kern, *Nano Lett.*, 2008, **8**, 4603–4607.
22 H. Liu, Y. Liu and D. Zhu, *J. Mater. Chem.*, 2011, **21**, 3335–3345.
23 A. Das, S. Pisana, B. Chakraborty, S. Piscanec, S. K. Saha, U. V. Waghmare, K. S. Novoselov, H. R. Krishnamurthy, A. K. Geim, A. C. Ferrari and A. K. Sood, *Nat. Nanotechnol.*, 2008, **3**, 210–215.
24 L. Tapasztó, G. Dobrik, P. Nemes-Incze, G. Vertesy, P. Lambin and L. P. Biró, *Phys. Rev. B: Condens. Matter Mater. Phys.*, 2008, **78**, 233407.
25 P. Venezuela, M. Lazzeri and F. Mauri, *Phys. Rev. B: Condens. Matter Mater. Phys.*, 2011, **84**, 035433.
26 R. Wang, S. Wang, D. Zhang, Z. Li, Y. Fang and X. Qiu, *ACS Nano*, 2010, **5**, 408–412.
27 Y. Sonnefraud, N. Verellen, H. Sobhani, G. A. E. Vandenbosch, V. V. Moshchalkov, P. Van Dorpe, P. Nordlander and S. A. Maier, *ACS Nano*, 2010, **4**, 1664–1670.
28 L. Ju, B. Geng, J. Horng, C. Girit, M. Martin, Z. Hao, H. A. Bechtel, X. Liang, A. Zettl, Y. R. Shen and F. Wang, *Nat. Nanotechnol.*, 2011, **6**, 630–634.
29 J. Niu, Y. J. Shin, Y. Lee, J.-H. Ahn and H. Yang, *Appl. Phys. Lett.*, 2012, **100**, 061116.
30 N. Papasimakis, Z. Luo, Z. X. Shen, F. De Angelis, E. Di Fabrizio, A. E. Nikolaenko and N. I. Zheludev, *Opt. Express*, 2010, **18**, 8353–8359.
31 N. K. Emani, T.-F. Chung, X. Ni, A. V. Kildishev, Y. P. Chen and A. Boltasseva, *Nano Lett.*, 2012, **12**, 5202–5206.
32 F. Wang, Y. Zhang, C. Tian, C. Girit, A. Zettl, M. Crommie and Y. R. Shen, *Science*, 2008, **320**, 206–209.
33 Z. Q. Li, E. A. Henriksen, Z. Jiang, Z. Hao, M. C. Martin, P. Kim, H. L. Stormer and D. N. Basov, *Nat. Phys.*, 2008, **4**, 532–535.
34 K. F. Mak, M. Y. Sfeir, Y. Wu, C. H. Lui, J. A. Misewich and T. F. Heinz, *Phys. Rev. Lett.*, 2008, **101**, 196405.
35 F. Schedin, A. K. Geim, S. V. Morozov, E. W. Hill, P. Blake, M. I. Katsnelson and K. S. Novoselov, *Nat. Mater.*, 2007, **6**, 652–655.
36 X. Gan, K. F. Mak, Y. Gao, Y. You, F. Hatami, J. Hone, T. F. Heinz and D. Englund, *Nano Lett.*, 2012, **12**, 5626–5631.